Applied Surface Science 442 (2018) 185–188

Contents lists available at ScienceDirect

Applied Surface Science

journal homepage: www.elsevier.com/locate/apsusc

Full Length Article

Effect of uniaxial stress on the electrochemical properties of graphene with point defects

Paweł Szroeder [a,*], Igor Yu. Sagalianov [b], Taras M. Radchenko [c], Valentyn A. Tatarenko [c], Yuriy I. Prylutskyy [d], Włodzimierz Strupiński [e,f]

[a] Institute of Physics, Kazimierz Wielki University, Powstańców Wielkopolskich 2, 85-090 Bydgoszcz, Poland
[b] Dept. of General Physics, Physical Faculty, Taras Shevchenko National University of Kyiv, 64 Volodymyrska Street, 01601 Kyiv, Ukraine
[c] Dept. of Metallic State Theory, G. V. Kurdyumov Institute for Metal Physics of the N.A.S. of Ukraine, 36 Academician Vernadsky Boulevard, 03142 Kyiv, Ukraine
[d] Dept. of Biophysics and Medical Informatics, ESC "Institute of Biology and Medicine", Taras Shevchenko National University of Kyiv, 64 Volodymyrska Street, 01601 Kyiv, Ukraine
[e] Faculty of Physics, Warsaw University of Technology, Koszykowa 75, 00-662 Warszawa, Poland
[f] Institute of Electronic Materials Technology, Wólczyńska 133, 01-919 Warszawa, Poland

ARTICLE INFO

Article history:
Received 27 October 2017
Revised 18 January 2018
Accepted 14 February 2018
Available online 15 February 2018

Keywords:
Graphene
Uniaxial strain
Point defects
Density of states
Heterogeneous electron transfer

ABSTRACT

We report a calculational study of electron states and the resulting electrochemical properties of uniaxially strained graphene with point defects. For this study the reduction of ferricyanide to ferrocyanide serves as a benchmark electrochemical reaction. We find that the heterogeneous electron transfer activity of the perfect graphene electrode rises under uniaxial strain. However, evolution of the cathodic reaction rate depends on the direction of strain. For moderate lattice deformations, the zigzag strain improves electrochemical performance better than the armchair strain. Standard rate constant increases by 50% at the zigzag strain of 10%. Vacancies, covalently bonded moieties, charged adatoms and substitutional impurities in the zigzag strained graphene induce changes in the shape of the curve of the cathodic reaction rate. However, this changes do not translate into the electrocatalytic activity. Vacancies and covalently bonded moieties at concentration of 0.1% do not affect the electrochemical performance. Charged adatoms and substitutional impurities give a slight increase in the standard rate constant by, respectively, 2.2% and 3.4%.

1. Introduction

Graphene, being a two-dimensional material without bulk, is extremely sensitive to the environment. This makes graphene a promising platform for a construction of electrochemical devices [1,2]. Electrocatalytic activity of graphene is strongly linked to the electron band structure, which is very sensitive to both the carbon honeycomb lattice deformations as well as defects.

Several strategies of tailoring graphene electronic structure for specific applications have been proposed: cutting graphene planes into nanoribbons [3,4], introducing of impurities and structural defects [5,6], ordering of the impurities [7–9], chemical functionalization [10], using of the substrate [11,12] as well as applying of the strain [13–15].

Among all the mentioned above approaches, the most promising is the use of strain, which is the most controllable and efficient way for tuning of the graphene electronic structure. Graphene, having an intrinsic tensile strength of 130 GPa and Young's modulus of about 1 TPa [9], withstands nondestructive deformations up to its failure strain of ≈25–27% [16,17]. Strain may arise spontaneously in graphene or can be intentionally induced and controlled with measurable effects [13] *via* different techniques [18,19].

Currently, the detailed mechanism of heterogeneous electron transfer between graphene electrode and electrolyte ions involving the strain combined with point defects remains vague. To address this question we perform simulations of the electrode reaction kinetics at graphene with point defects combined with uniaxial stress. We consider such defects as: (1) covalently bonded moieties (e.g. H, OH, CH_3, CH_2OH, C_2H_5OH) represented by resonant impurities (RIs), (2) vacancies (Vs), (3) charged adatoms (e.g. alkali and the group III metals) represented by Gaussian impurities (GIs), and (4) substitutional impurities represented by Gaussian hoppings (GHs). In calculations we use the $Fe(CN)_6^{3-/4-}$ redox couple as an electrochemical probe.

* Corresponding author.
E-mail address: psz@ukw.edu.pl (P. Szroeder).

https://doi.org/10.1016/j.apsusc.2018.02.150
0169-4332/

2. Models

Electronic density of states (DOS) for graphene was calculated using the standard p-orbital nearest-neighbor tight-binding Hamiltonian $\widehat{H} = -\gamma_0^1 \sum_{i,i'} c_i^\dagger c_{i'} + \sum_i V_i c_i^\dagger c_i$, where $c_i^\dagger$ (c_i) was a standard creation (annihilation) operator acting on a quasiparticle at the site i [20]. The summation over i ran the entire honeycomb lattice, while i' was restricted to the sites next to i; $\gamma_0^1 = 2.78$ eV was the hopping integral for the nearest-neighbor graphene-lattice sites at a distance $a = 0.142$ nm (C—C bond length in graphene). V_i was the on-site potential defining scattering strength on graphene-lattice site i due to the point defect presence.

Following Refs. [14,21,22], where random strain was modeled by the Gaussian function, it was assumed a dependence of the bond lengths on the deformation tensor components. Hopping parameters of the strained graphene, γ, were related with hopping of the unstrained lattice, γ_0^1, using the exponential decay $\gamma(l) = \gamma_0^1 e^{-\beta(l/a-1)}$, where l was a C—C bond length under the strain, and $\beta \approx 3.37$ was a decay rate extracted from experiments [21,23].

Modeling of RIs was carried out with the Hamiltonian part proposed by Huan et al. [20] $\widehat{H}_{\text{imp}} = \chi_d \sum_i^{N_{\text{imp}}} d_i^\dagger d_i + V \sum_i^{N_{\text{imp}}} (d_i^\dagger c_i + \text{H.c.})$, where N_{imp} denoted number of the RI. Band parameters $V \approx 2\gamma_0^1$ and $\chi_d \approx -\gamma_0^1/16$ were obtained from density-functional theory calculations [24]. Vacancies were modeled as empty sites of graphene lattice with hopping parameters to other sites being zero.

GIs were represented by Gaussian-like scattering potential $V_i = \sum_{j=1}^{N_{\text{imp}}^V} U_j \exp\left(-|\mathbf{r}_i - \mathbf{r}_j|^2/(2\xi^2)\right)$, where $\mathbf{r}_i$ was the radius-vector of the i site, $\mathbf{r}_j$ defined position of the N_{imp}^V impurity atoms, ξ was interpreted as an effective potential radius. Potential height U_j was uniformly random in the range $[-\triangle, \triangle]$ with $\triangle$ being the maximum potential height [20]. In the calculations we considered short-range GI (SRGI) with values of $\xi = 0.65a$ and $\triangle = 3\gamma_0^1$ and long-range GI (LRGI) with $\xi = 5a$, $\Delta = \gamma_0^1$.

GHs modified a distribution of the hopping integrals $\gamma_{i,j} = \gamma + \sum_{k=1}^{N_{\text{hop}}^\gamma} U_k^\gamma \exp\left(-|\mathbf{r}_i + \mathbf{r}_j - 2\mathbf{r}_k|^2/(8\xi_\gamma^2)\right)$, [20]. Here, $\mathbf{r}_i$ and $\mathbf{r}_j$ were radius-vectors of graphene sites, $\mathbf{r}_k$ defined position of the strain centers, N_{hop}^γ defined their number, ξ_γ was considered as an effective screening length, and hopping height $U_k^\gamma \in [-\triangle_\gamma, \triangle_\gamma]$. Effective screening length for short-range GH (SRGH) was assumed to be $\xi_\gamma = 0.65a$, maximal hopping height was $\Delta_\gamma = 1.5\gamma_0^1$. For long-range GH (LRGH), $\xi_\gamma = 5a$ and $\Delta_\gamma = 0.5\gamma_0^1$.

Numerical calculation of DOS was based on a computation of the first diagonal element of the Green's function using continued fraction technique and tridiagonalization procedure of the Hamiltonian matrix (see details in Appendix of Ref. [25]).

Electron transfer rate for cathodic reaction, k_c, was calculated using the Gerischer-Marcus model [26] applied to the sp^2 carbon systems [7,27]. Cathodic reaction rate, k_c, was calculated using the integral $k_c(E) \propto \int f(\epsilon - eE)\, \rho(\epsilon - eE)\, W_{\text{Ox}}(\epsilon)\, d\epsilon$,in which distributions of the filled states of graphene electrode, $f(\epsilon - eE)\, \rho(\epsilon - eE)$, and the unoccupied states of the oxidized form in the solution, $W_{\text{Ox}}(\epsilon)$, were considered. Here, $f(\epsilon - eE)$ was the Fermi-Dirac distribution at a specified electrode potential E. Distribution of electron states of the oxidized form in the solution was defined by $W_{\text{Ox}}(\epsilon) = (4\pi\lambda k_B T)^{-1/2} \exp\left[-(\epsilon - \epsilon_{\text{F,redox}} - \lambda)^2/4\lambda k_B T\right]$, where k_B was the Boltzmann constant, T was the absolute temperature, $\epsilon_{\text{F,redox}}$ was the Fermi level of the redox couple with respect to the graphene charge neutrality level, λ was the reorganization energy. We performed simulations for reduction of the $Fe(CN)_6^{3-}$, for which $\lambda = 0.7$ eV [28] and $\epsilon_{\text{F,redox}} = -1.27$ eV [27]. To estimate the standard rate constant for the $Fe(CN)_6^{3-/4-}$ redox couple, we assumed the standard electrode potential of 0.29 V *vs.* Ag/AgCl obtained from half-wave potential in cyclic voltammetry experiments.

3. Results and discussion

Calculations carried out for perfect graphene lattice indicate a strong dependence of DOS on the strain direction. In the inset of Fig. 1(a) an evolution of DOS under the armchair uniaxial strain is presented. Linear dependence of DOS on energy is preserved near the charge neutrality level. The slope of DOS increases with the increasing armchair strain and an extra pair of the van Hove singularities appears. The singularities shift towards charge neutrality level with increasing strain.

Cathodic reaction rate for reduction of the $Fe(CN)_6^{3-}$ at graphene is not a monotonically increasing function of the electrode potential. Due to the low DOS near the charge neutrality level, we observe in the plots a valley above the local maximum. As we show in Fig. 1a, the armchair strain boosts the heterogeneous electron transfer kinetics – the hump increases with increasing strain. Under the strain of 25% another hump emerges at 0.15 eV, which results from the electrode states from the van Hove singularities approaching to the charge neutrality level.

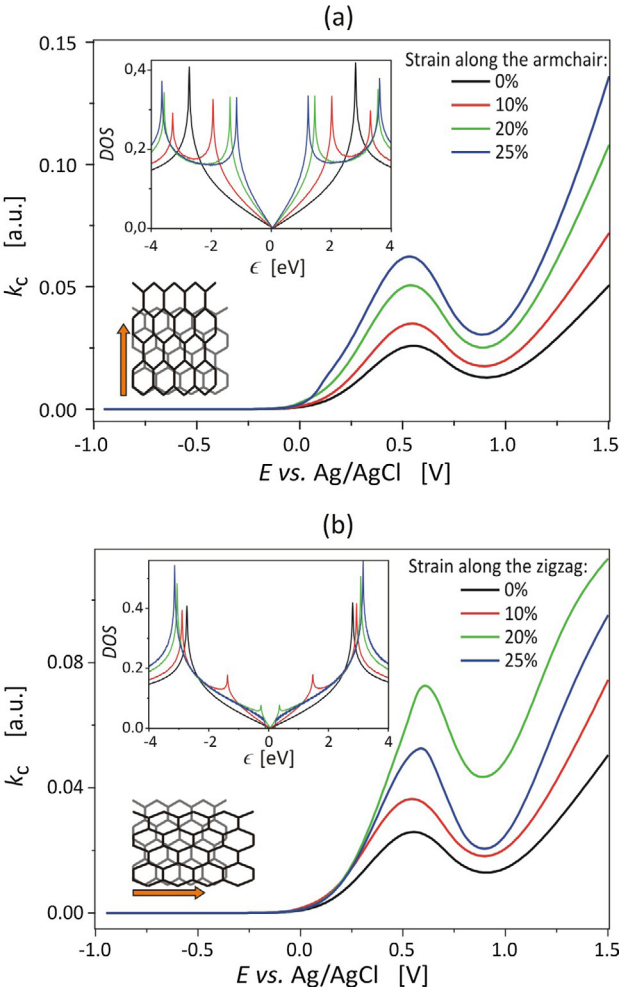

Fig. 1. Curves of the cathodic reaction rate for reduction of the $Fe(CN)_6^{3-}$ at the perfect graphene electrode subjected to uniaxial strain. In the insets, the calculated DOS of perfect graphene under strain are shown. (a) Uniaxial strain along the armchair direction. (b) Strain along the zigzag direction.

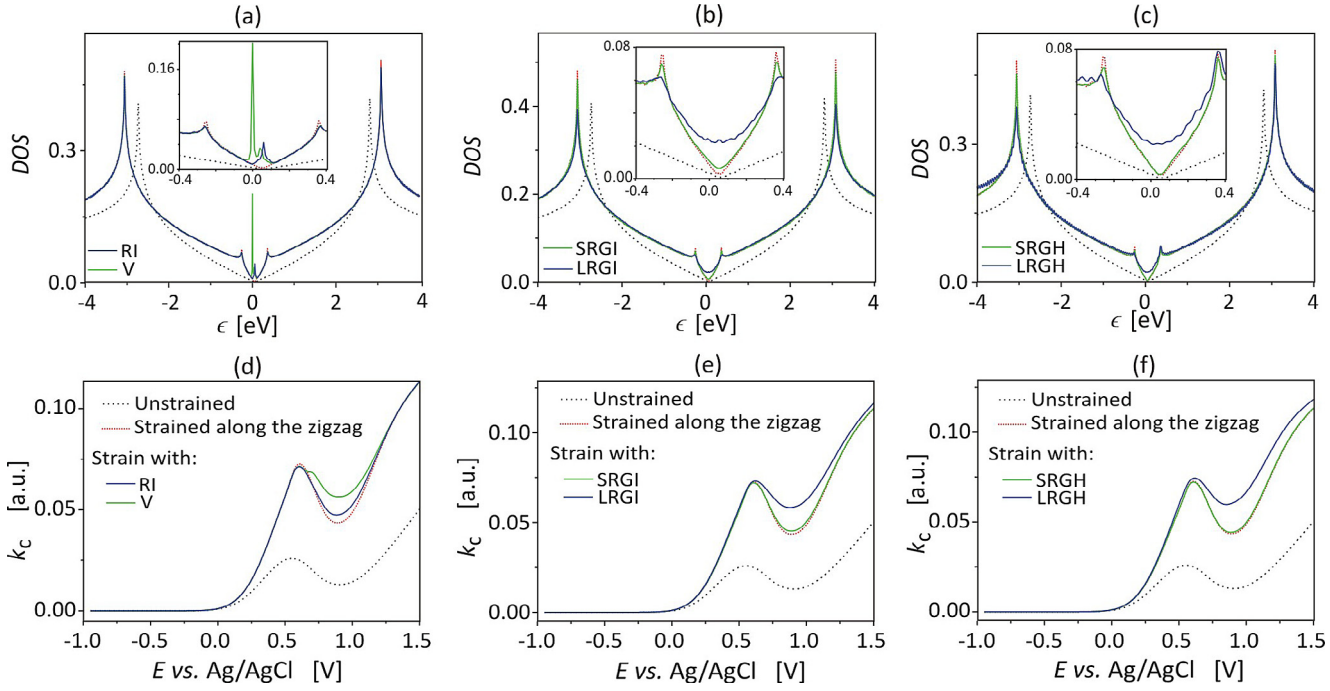

Fig. 2. (a–c) DOS of graphene under the zigzag strain of 20% with different point defects at the fixed concentration of 0.1%. In the insets of the a–c panels, the DOS near the charge neutrality point is shown. (d–f) Corresponding plots of the cathodic reaction rate for reduction of the $Fe(CN)_6^{3-}$.

When we apply the uniaxial strain along the zigzag direction, the van Hove singularity-like peaks appear in DOS as well (inset of Fig. 1(b)). But they shift fast into the charge neutrality level with increasing strain and finally disappear. Under the zigzag strain, the DOS spectrum loses its linear dependence near the charge neutrality level. Higher strain induces the band gap opening. Width of the band gap increases with increasing strain and achieves a value of 0.35 eV under the strain of 25%. The moderate zigzag strain facilitates the heterogeneous electron transfer better than the armchair strain. As we see in Fig. 1(b), the hump in the curve of the cathodic reaction rate builds up faster than under the armchair strain. However at higher values of strain ($\geqslant$ 20%), electrode reaction rate declines due to the band gap.

Plots in Fig. 2(a)–(c) shows the influence of different point defects at a fixed concentration of 0.1% on DOS of graphene under the zigzag strain of 20%. Both the RIs and Vs induce additional electronic states which form narrow peaks near the charge neutrality level (Fig. 2(a)). However, Vs modify DOS more markedly than RIs. The V-induced states form two clearly distinguishable peaks. The stronger peak has intensity, which is nearly five times higher than intensity of the peak formed by the RI states. GIs (charged adatoms) and GHs (interstitial atoms) create smooth, quasi-continuous spectrum of states between the van Hove-like peaks induced by strain (Fig. 2 (b) and (c)). However DOS near the charge neutrality level is decaying drastically with decreasing of the (effective) screening length of defects. When the ξ (ξ_γ) value is lower than the C—C bond length, a, GIs and GHs contribute poorly to DOS.

Corresponding plots of the cathodic reaction rate are shown in Fig. 2(d)–(f). The defect states induced near the Fermi level lead to the shallowing of valleys above the humps in the curves. RIs in the zigzag strained graphene give slight contribution to the electrode reaction rate as compared with vacancies. Vacancies contribute not only to the decrease of the local minimum above the hump but also give rise to emerging another hump at 0.7 V *vs* Ag/AgCl (Fig. 2(d)). The best kinetics of the cathodic reaction ensures the strain combined with GIs and GHs, provided that the screening length is enough, *i.e.* ξ and $\xi_\gamma = 5a$ (Fig. 2(e) and (f)).

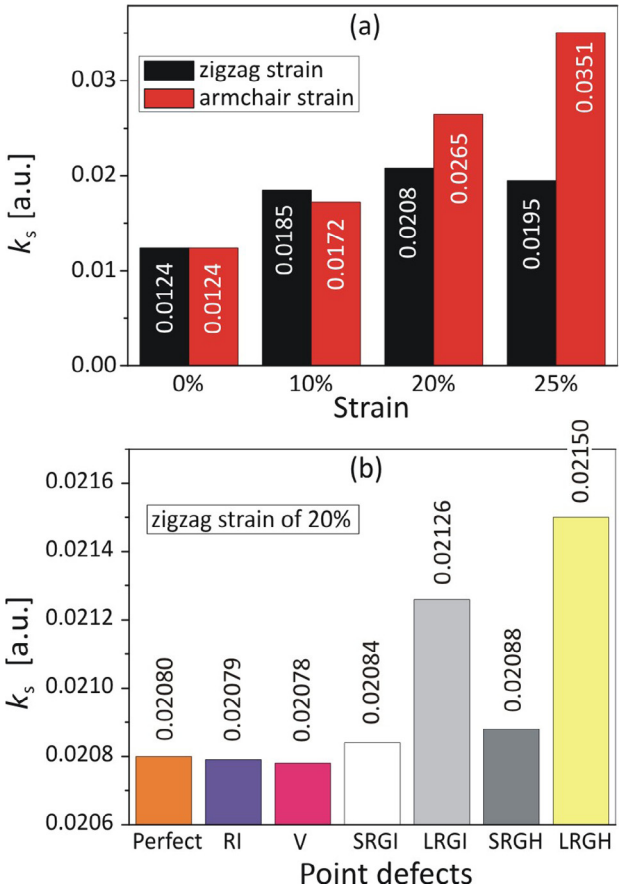

Fig. 3. (a) Calculated standard electron transfer rate constants for the $Fe(CN)_6^{3-/4-}$ redox couple at the perfect graphene electrode under the strain. (b) Comparison of the standard rate constants at graphene electrode under the zigzag strain of 20% with different types of point defects at fixed concentration of 0.1%.

We would like to point out that LRGHs are slightly more effective in the increasing of the reaction rate than the LRGIs.

Calculated relative standard electron transfer rate constants, k_s, at the perfect graphene electrode under the uniaxial strain for the $Fe(CN)_6^{3-/4-}$ redox couple are compared in Fig. 3. When the strain is applied along the armchair direction, we observe monotonic increase of the standard rate constant up to the strain of 25%. The value of k_s at graphene electrode stretched by 25% is more than three times higher than in the unstrained graphene. For moderate strain (<20%), deformation along the zigzag direction causes a faster increase of the k_s compared to the armchair strain. Standard rate constant increases by half at the zigzag strain of 10%. Under higher strain, band gap hinders a fast growth of the k_s.

The values of k_s for the $Fe(CN)_6^{3-/4-}$ redox couple at the zigzag strained graphene electrode with different point defects are compared in Fig. 3(b). We see very limited impact of defects on electrocatalytic performacne towards $Fe(CN)_6^{3-/4-}$ redox reaction, at least at the considered defect concentration of 0.1%. Introduction of the LRGI and LRGH into the strained graphene lattice causes, respectively, a 2.2% and 3.4% increase in the electron transfer rate constant. RIs and Vs do not improve the k_s value, but rather somewhat diminish it by less than 0.1%. Such difference is due to the character of the defect induced electron DOS spectrum. In general, narrow peaks created by RIs and Vs in DOS do not facilitate electrochemical performance. An advantage of introduction of substitutional impurities represented by LRGHs over covalent functionalization (RIs) is already confirmed in experiments with graphene doped with nitrogen [29] and boron [30]. However, in that experiments the effect of strain is not considered.

4. Conclusions

We show that the uniaxial strain has a strong impact on the heterogeneous electron transfer kinetics between the graphene electrode and the $Fe(CN)_6^{3-/4-}$ redox couple. For moderate deformations (<20%), the perfect graphene under the zigzag strain exhibits better electrocatalytic activity than the armchair strained graphene. Stretching of graphene electrode by 10% along zigzag direction results in 50% increase of the electron transfer standard rate constant.

On the other hand, we see rather limited impact of defects introduced into the strained graphene on the electrocatalytic performance towards the $Fe(CN)_6^{3-/4-}$ redox reaction. Although the defect states result in the shallowing of valleys above the humps in the curves of the cathodic reaction rate, the standard rate constant rises poorly. The most promising defects, i.e. GIs (charged adatoms) and GHs (substitutional impurities) with large enough screening length of several C—C bond lengths and concentration of 0.1%, induce the increase in the standard rate constant by 2.2% and 3.4%, respectively. Vacancies and RIs at the same concentrations do not make any contribution to the electrocatalytic performance towards the $Fe(CN)_6^{3-/4-}$ redox reaction.

Acknowledgements

This work was financed by Institute of Physics, Kazimierz Wielki University – Poland, Dept. of General Physics, Taras Shevchenko National University of Kyiv – Ukraine, and G.V. Kurdyumov Institute for Metal Physics of the N.A.S.U. – Ukraine from funds for statutory research. Authors acknowledge the Polish-Ukrainian joint research project under the agreement on scientific cooperation between the Polish Academy of Sciences and the National Academy of Sciences of Ukraine for 2015–2017 (No. 793). The authors would like to thank Taras Shevchenko National University of Kyiv for providing an opportunity to use its computational cluster resources for DOS calculations.

References

[1] A.K. Geim, K.S. Novoselov, The rise of graphene, Nat. Mater. 6 (3) (2007) 183–191.
[2] A. Ambrosi, C.K. Chua, A. Bonanni, M. Pumera, Electrochemistry of graphene and related materials, Chem. Rev. 114 (14) (2014) 7150–7188.
[3] M. Han, B. Ozyilmaz, Y. Zhang, P. Kim, Energy band-gap engineering of graphene nanoribbons, Phys. Rev. Lett. 98 (20) (2007) 206805-1–206805-4.
[4] W. Jaskólski, A. Ayuela, M. Pelc, H. Santos, L. Chico, Edge states and flat bands in graphene nanoribbons with arbitrary geometries, Phys. Rev. B 83 (23) (2011) 235424-1–235424-9.
[5] D.C. Elias, R.R. Nair, T.M.G. Mohiuddin, S.V. Morozov, P. Blake, M.P. Halsall, A.C. Ferrari, D.W. Boukhvalov, M.I. Katsnelson, A.K. Geim, K.S. Novoselov, Control of graphene's properties by reversible hydrogenation: evidence for graphane, Science 323 (5914) (2009) 610–613.
[6] F. Ouyang, S. Peng, Z. Liu, Z. Liu, Bandgap opening in graphene antidot lattices: the missing half, ACS Nano 5 (5) (2011) 4023–4030.
[7] T.M. Radchenko, V. Tatarenko, I. Sagalianov, Y.I. Prylutskyy, P. Szroeder, S. Biniak, On adatomic-configuration-mediated correlation between electrotransport and electrochemical properties of graphene, Carbon 101 (2016) 37–48.
[8] T.M. Radchenko, V.A. Tatarenko, Kinetics of atomic ordering in metal-doped graphene, Solid State Sci. 12 (2) (2010) 204–209.
[9] T.M. Radchenko, V.A. Tatarenko, A statistical-thermodynamic analysis of stably ordered substitutional structures in graphene, Physica E 42 (8) (2010) 2047–2054.
[10] T. Sainsbury, M. Passarelli, M. Naftaly, S. Gnaniah, S.J. Spencer, A.J. Pollard, Covalent carbene functionalization of graphene: Toward chemical band-gap manipulation, ACS Appl. Mater. Inter. 8 (7) (2016) 4870–4877.
[11] S.Y. Zhou, G.H. Gweon, A.V. Fedorov, P.N. First, W.A. de Heer, D.H. Lee, F. Guinea, A.H. Castro Neto6, A. Lanzara, Substrate-induced bandgap opening in epitaxial graphene, Nat. Mater. 6 (2007) 770–775.
[12] J. Jung, A.M. DaSilva, A.H. MacDonald, S. Adam, Origin of band gaps in graphene on hexagonal boron nitride, Nat. Commun. 6 (2015) 6308-1–6308-11.
[13] Z.H. Ni, T. Yu, Y.H. Lu, Y.Y. Wang, Y.P. Feng, Z.X. Shen, Uniaxial strain on graphene: Raman spectroscopy study and band-gap opening, ACS Nano 2 (11) (2008) 2301–2305.
[14] V.M. Pereira, A.H.C. Neto, Strain engineering of graphene's electronic structure, Phys. Rev. Lett. 103 (4) (2009) 046801-1–046801-4.
[15] I.Y. Sagalianov, T.M. Radchenko, Y.I. Prylutskyy, V.A. Tatarenko, P. Szroeder, Mutual influence of uniaxial tensile strain and point defect pattern on electronic states in graphene, Eur. Phys. J.B 90 (6) (2017) 112-1–112-9.
[16] C. Lee, X. Wei, J.W. Kysar, J. Hone, Measurement of the elastic properties and intrinsic strength of monolayer graphene, Science 321 (5887) (2008) 385–388.
[17] E. Cadelano, P.L. Palla, S. Giordano, L. Colombo, Nonlinear elasticity of monolayer graphene, Phys. Rev. Lett. 102 (23) (2009) 235502-1–235502-4.
[18] C. Si, Z. Sun, F. Liu, Strain engineering of graphene: a review, Nanoscale 8 (2016) 3207–3217.
[19] B. Amorim, A. Cortijo, F. de Juan, A.G. Grushin, F. Guinea, A. Gutierrez-Rubio, H. Ochoa, V. Parente, R. Roldan, P. San-Jose, J. Schiefele, M. Sturla, M.A.H. Vozmediano, Novel effects of strains in graphene and other two dimensional materials, Phys. Rep. 617 (2016) 1–54.
[20] S. Yuan, H. De Raedt, M.I. Katsnelson, Modeling electronic structure and transport properties of graphene with resonant scattering centers, Phys. Rev. B 82 (11) (2010) 115448-1–115448-16.
[21] R.M. Ribeiro, V.M. Pereira, N.M.R. Peres, P.R. Briddon, A.H. Castro Neto, Strained graphene: tight-binding and density functional calculations, New J. Phys. 11 (2009) 115002-1–115002-10.
[22] B. Burgos, J. Warnes, L.R.F. Leandro Lima, C. Lewenkopf, Effects of a random gauge field on the conductivity of graphene sheets with disordered ripples, Phys. Rev. B. 91 (11) (2015) 115403-1–115403-10.
[23] A.H. Castro Neto, F. Guinea, Electron-phonon coupling and raman spectroscopy in graphene, Phys. Rev. B 75 (4) (2007) 045404-1–045404-8.
[24] T.O. Wehling, S. Yuan, A.I. Lichtenstein, A.K. Geim, M.I. Katsnelson, Resonant scattering by realistic impurities in graphene, Phys. Rev. Lett. 105 (5) (2010) 056802-1–056802-4.
[25] T.M. Radchenko, A.A. Shylau, I.V. Zozoulenko, Influence of correlated impurities on conductivity of graphene sheets: time-dependent real-space Kubo approach, Phys. Rev. B 86 (3) (2012) 035418-1–035418-13.
[26] H. Gerischer, Physical Chemistry: An Advanced Treatise, first ed., vol. 9A, Academic Press, Inc., New York, 1970.
[27] P. Szroeder, Electron transfer kinetics at single-walled carbon nanotube paper: the role of band structure, Phys. E 44 (2011) 470–475.
[28] H. Morisaki, H. Ono, K. Yazawa, Electronic state densities of aquo-complex ions in water determined by electrochemical tunneling spectroscopy, J. Electrochem. Soc. 136 (6) (1989) 1710–1714.
[29] K.P. Prathish, M.M. Barsan, D. Geng, X. Sun, C.M. Brett, Chemically modified graphene and nitrogen-doped graphene: electrochemical characterisation and sensing applications, Electrochim. Acta 114 (2013) 533–542.
[30] Y. Xu, W. Lei, Z. Han, T. Wang, M. Xia, Q. Hao, Boron-doped graphene for fast electrochemical detection of HMX explosive, Electrochim. Acta 216 (2016) 219–227.